JASA ARTICLE

Improving onset picking in ultrasonic testing by using a spectral entropy criterion

Benjamin Bühling[a] and Stefan Maack
Bundesanstalt für Materialforschung und -prüfung (BAM), Berlin 12205, Germany

ABSTRACT:
In ultrasonic testing, material and structural properties of a specimen can be derived from the time-of-flight (ToF). Using signal features, such as the first peak or envelope maximum, to calculate the ToF is error-prone in multipath arrangements or dispersive and attenuating materials, which is not the case for the signal onset. Borrowing from seismology, researchers used the Akaike information criterion (AIC) picker to automatically determine onset times. The most commonly used formulation, Maeda's AIC picker, is reassessed and found to be based on inappropriate assumptions for signals often used in ultrasonic testing and dependent on arbitrary parameters. Consequently, an onset picker for ultrasonic through-transmission measurements is proposed, based on a spectral entropy criterion (SEC) to model the signal using the AIC framework. This SEC picker takes into account the spectral properties of the ultrasonic signal and is virtually free of arbitrary parameters. Synthetic and experimental data are used to compare the performance of SEC and AIC pickers. It is shown that the accuracy of onset picking is improved for densely sampled data.
https://doi.org/10.1121/10.0024337

(Received 3 July 2023; revised 13 December 2023; accepted 15 December 2023; published online 23 January 2024)

[Editor: Julien de Rosny] Pages: 544–554

I. INTRODUCTION

Time-of-flight (ToF) analysis of an acoustic signal is a prominent method of investigation in various scientific domains. Applications include the analysis of earthquakes in geophysics,[1] the prediction of avalanches in glaciology,[2] the localization of cracks in concrete structures by acoustic emission testing,[3] or ultrasonic imaging, both in medical applications[4,5] and in nondestructive testing.[6] In this list of acoustic ToF applications, ultrasonic testing differs from the remaining ones because the properties of the analyzed acoustic signal are generally known in advance. When performing ToF measurements, the received ultrasonic pulse is usually compared to a reference pulse, which may be modeled[7] or measured directly.[8] This comparison may involve waveform cross correlation[9] or identification of shifts in certain waveform properties, including first maximum, first zero crossing, first threshold crossing, or signal onset.[10] However, with the exception of the signal onset, using these properties for ToF measurements can lead to erroneous results if the pulse propagates through an attenuating and dispersive medium. In this case, the waveform of broadband pulses changes according to the distance traveled and frequency content, since dispersivity causes the frequency components to propagate at different phase velocities while attenuation affects higher frequency components more than lower frequency components.[11] The signal onset is considered to be a characteristic waveform property that is largely unaffected by these effects.[12,13] Furthermore, signal onset is the only signal feature that reliably indicates the shortest travel path through a material, which is particularly important in air-coupled ultrasonic testing where a large difference exists between the propagation velocities in air and specimen.[14] However, the true value of the signal onset is difficult to determine in measured signals because it is always hidden in background noise.

The most common method for finding a signal onset in ultrasonic testing is the *Akaike information criterion picker* (AIC picker).[4,6,13,15,16] It is based on an information criterion developed by Akaike[17] to compare various statistical models in terms of error and complexity. It was later transferred to geophysical applications[18,19] to separate waveform segments that can be described by different models, which includes onset picking. In this domain, it has been shown to outperform previous methods, such as the often used short-term average/long-term average (LTA/STA) technique[20,21] or the threshold method.[22] Following the rediscovery of Maeda's[23] simplified approach to the AIC picker 2 decades ago,[24,25] it has become a relevant reference method for benchmarking of newly developed methods.[26–28] This success is likely a result of the fact that the algorithm does not require *a priori* knowledge about neither signal properties and measurement setup and is easy to implement. The importance of Maedas' AIC Picker is reflected in the fact that many of the newly developed methods are adaptations of the AIC Picker[4,6,22,29–32] or recombine it with other onset picking methods.[21,33–35] Further onset picking methods rely, for example, on edge enhancement filter[36] or continuous

[a]Email: benjamin.buehling@bam.de

https://doi.org/10.1121/10.0024337

wavelet transforms[37] and have been comprehensively reviewed by Das and Leung.[30] More recently, deep learning models[38] have been proposed for onset detection, which provide better results but are more difficult to implement because they require extensive training on large domain-specific datasets.

Using the signal properties available in ultrasonic testing, this paper proposes a novel signal onset picker designed primarily for ultrasonic through-transmission applications. In Sec. II, the AIC picker is revisited with a special focus on Maeda's formulation. Both general implications and the particular ones concerning ultrasonic measurements that are resulting from this formulation are discussed. Building on this discussion, Sec. III introduces the spectral entropy criterion (SEC) picker as a novel method that is methodologically based on the AIC picker. However, instead of relying on signal variance, a spectral entropy model is used to detect a pulse onset. In Sec. IV, the synthetic and experimental data are described, that are used in Sec. V to compare the behavior of the AIC picker and the SEC picker and assess the influence of various parameters on the method to define its limitations. With this knowledge, the SEC picker is then applied to experimental data to evaluate its performance in comparison to the AIC picker.

II. AKAIKE INFORMATION CRITERION PICKER

The AIC was initially developed to compare and select statistical models and is still an important tool for this purpose.[17,39,40] The criterion is defined as

$$\mathrm{AIC} = -2\ln(L) + 2p, \tag{1}$$

where L is the likelihood of the estimated model and p is the number of model parameters. When comparing different models, the model with the lowest AIC best represents a given distribution, making the latter term a penalty term.

If a time signal contains two distinct segments, these can be interpreted as two distributions that can be modeled. The best possible approximation of the signal is achieved when both models fit the distribution. To do this, they must predict their waveform segment well and must only be compared to the corresponding waveform segment. The error increases when a model is compared to a waveform partition that includes a set of values belonging to a segment with a different distribution. Thus, the signal is best separated when both models appropriately represent the segment distributions and are compared to waveform segments that include the fewest data points belonging to the respective other distribution. For predefined models, each possible separation point is tested using Eq. (1). Using the log-likelihood, the AIC at a tested separation point k in the interval $[1,N]$ is

$$\mathrm{AIC}(k) = k\log(\sigma_1^2) + (N-k)\log(\sigma_2^2), \tag{2}$$

with mean squared error (MSE) σ_i^2 of the segment models $\hat{s}$ compared to the actual data s at points j:

$$\sigma_i^2 = \mathrm{mean}\{(s(t) - \hat{s}(t))^2\}. \tag{3}$$

These are evaluated in the interval $t = [1, k-1]$ for $i = 1$ and in the interval $t = [k, N]$ for $i = 2$. A detailed derivation of Eq. (2) can be found in the original paper by Kitagawa and Akaike[18] as well as in a number of subsequent publications.[3,19] As the AIC value is calculated for an increasing index k, the first term in Eq. (2) can be interpreted as a forward running function (FW) since the window size in which σ_1 is calculated increases. Accordingly, the second term can be interpreted as a backward running function (BW).[41] A schematic representation of these functions and windows is given in Fig. 1. If the first model fits the behavior of the first segment of the time signal, the FW function gives a constant low or continuously decreasing result. As the FW windows are increased beyond the true separation point, the error increases and so does the result of the FW function. The BW function behaves accordingly: it starts with a high output when data points from the first segment are included in the window and decreases to a constant low value when only points from the second segment are included. The addition of the FW and BW functions, according to Eq. (2), leads to a global minimum at the optimum separation point.[41]

In geophysical applications, where the AIC picker was used to determine onset times and distinguish wave modes in the years following its original publication, the waveform segments were usually modeled as autoregressive functions.[18,19,41] Accordingly, it was termed an autoregressive AIC (AR-AIC) picker.[25,42] The only exception was Maeda,[23] who published a Japanese-language paper that is available to the author as a machine-translated version. This paper included a modification of Eq. (2), that attempted to model both signal segments as Gaussian processes. Thus, Maeda's AIC picker is defined as

$$\begin{aligned}\mathrm{AIC}_M(k) = {} & k\log(\mathrm{var}\{s(t=[1,k-1])\}) \\ & + (N-k)\log(\mathrm{var}\{s(t=[k,N])\}),\end{aligned} \tag{4}$$

where $\mathrm{var}\{s(t)\}$ is the empirical variance of the waveform calculated for each segment before and after separation point k. Although Maeda found that this approach was beneficial for noisy data, Eq. (4) was not referred to for more than a decade. Following its rediscovery in 2003,[24,25] Maeda's AIC picker has become the predominant version of the AIC picker and will be used below under the name *AIC*

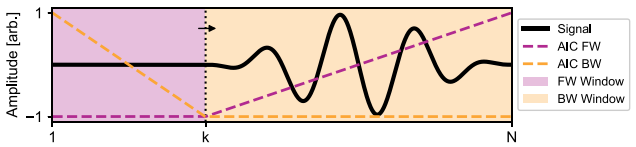

FIG. 1. (Color online) Schematic representation of the Akaike information criterion (AIC) picker. As k is moved across the entire waveform, the FW and BW functions are calculated for the signal segments preceding and following k, respectively. When these functions are added, the global minimum gives the signal onset predicted by the AIC.

picker. Compared to the AR-AIC picker, it has the distinct advantage that it does not require prior modeling of the signal segments. Thus, Eq. (4) can be applied to any signal without prior knowledge or model optimization.

The difference in Eqs. (2) and (4) is the variance terms. While in Eq. (2) the MSE σ_i^2 describes the error of the segment model compared to the actual data, empirical variance in Eq. (4) describes the mean squared deviation of the data from its mean in the respective interval. Therefore, in terms of the original AIC picker, the model employed in Eq. (4) to describe both signal segments is $\hat{s}(t) = \text{mean}\{s(t)\}$, which corresponds to $\hat{s}(t) = 0$ in most acoustic applications. Both signal segments are modeled identically, and this model is constant zero. In cases where the first signal segment contains only noise, this model is a useful approximation. However, more useful models are required for the second segment, whether it contains seismic activity or an ultrasonic pulse. Moreover, the use of an inappropriate model for the second signal segment results in a behavior of the AIC picker that deviates from its original theory. Since the first signal segment has only little variance and the second segment after the signal onset has higher variance, Maeda's BW function results in continuously increasing values in the first signal segment. For $k = 1$, the logarithmic variance of the BW function is calculated for the entire recorded signal. Figure 2 shows that as k is increased, lower variance samples in the signal are discarded from the BW function window and the overall logarithmic variance in the BW function increases with a slope, depending on the increase in variance and the length of the first signal segment. While the FW function generally behaves as expected, the BW function does not. As shown in Fig. 1, the BW function should complement the behavior of the FW function so that a global minimum is formed as both are added. The flawed modeling of the second signal segment is the reason that the BW function in Fig. 2 is monotonically increasing around the onset point instead of exhibiting a change of slope as the FW function does and as it is intended.

For the original AR-AIC picker, it has been proposed in the literature to use the FW function only and omit adding a BW function.[19,41] Figure 2 also suggests that this would be sufficient. However, for noisier signals than the one shown in Fig. 2, adding the BW function to the FW function paradoxically increases picking accuracy. Since the first segment's variance often increases noticeably only a few samples after the signal onset, the FW function's minimum is also often found a few samples behind the true signal onset. By adding a continuously increasing function, like the BW function, the overall AIC picker minimum is slightly shifted to earlier samples, which tends to increase picking accuracy. Despite being beneficial for the picking performance, this behavior is not intended in the design of the AIC picker. However, it demonstrates the complex interrelationship between segment variances and segment lengths, that influence the effect of this unintended behavior.

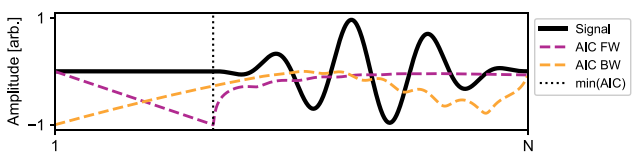

FIG. 2. (Color online) Behavior of Maeda's Akaike information criterion (AIC) picker when applied to a synthetic RCS4 pulse.

Given the ease of implementation and satisfying picking performance, these theoretical issues have been disregarded in the literature. However, several authors have addressed performance issues that are likely due to the simplifications used. The issue of poor onset picking accuracy in the presence of a low second derivative of the AIC, already mentioned by Maeda,[23] was proposed to be solved by filtering those values.[3] Furthermore, the signal onset picking accuracy depends on the number of samples in the waveform preceding and following the true signal onset. Both Kurz *et al.*[6] and Sedlak *et al.*[22] have proposed methods that adjust the waveform snippet size. However, both rely on empirical parameters based on experience and cannot be easily transferred to other domains and experimental setups without doing a form of parameter search and stability analysis. In addition to departing from the original zero-knowledge approach of Maeda's formulation, none of these improvements address the underlying issue of inappropriate signal modeling.

While passive acoustic methods have limited prior knowledge of the received signals, active methods, such as ultrasonic testing, rely on predetermined, reproducible, and deliberately chosen signal characteristics. Transducer properties, such as the frequency response, are therefore generally known in advance and should be included in the onset picking algorithm.

III. SPECTRAL ENTROPY CRITERION PICKER

The onset-picking algorithm proposed in this paper was developed to incorporate knowledge of the ultrasonic signal characteristics while preserving the desirable properties of the AIC picker. It does not require modeling of the signal or input of arbitrary empirical parameters.

In ultrasonic testing, especially in through-transmission setups, it is known that the signal spectrum before onset is significantly different from the spectrum after onset. In the first segment, the signal is dominated by white noise with a flat spectrum. In the second segment, the transmitted ultrasonic signal is generally characterized by a spectrum with a pronounced center frequency. The spectra of these two segments can be considered stationary in the sense that the flat spectrum of the first segment and the dominant frequency in the second segment do not change significantly across the segment width. Thus, the separation point between these constant spectrum segments marks the signal onset. In this paper, the normalized spectral entropy H_s is used as an indicator of a change in a spectrum. The resulting onset picking method is therefore termed the *spectral entropy criterion picker* (SEC picker). The spectral entropy is based on

https://doi.org/10.1121/10.0024337

Shannon's entropy H,[43] which, for a set of symbols X of size m with discrete probabilities p_i, is defined as

$$H = -\sum_{i=1}^{m} p_i \log_2(p_i). \tag{5}$$

It is a measure for the average information of each symbol in that set.[44] Signal onset pickers based on entropy measures have been presented before, but almost exclusively calculated entropy measures directly from the time signal rather than from its spectrum. Exceptions are da Silva and Corso,[45] who use the concept of spectral entropy in conjunction with the STA/LTA picker and Das *et al.* who used spectral entropy as an indicator for concrete damage[46] and healing[47] in acoustic emission testing. Calculating Shannon entropy directly from the waveform, however, poses a challenge. Given the typically high bit depth of measurements, a windowed signal taken from a single waveform usually includes insufficient samples to produce reliable statistics on its entropy. This contrasts with the number of possible unique frequency components obtained from a discrete Fourier transform (DFT), according to Eq. (7), which is half the window size if zero padding is not applied. To approximate waveform signal entropy, various contrast functions have been developed as part of independent component analysis (ICA).[48] These functions aim at determining the "Gaussianity" of a function and thereby its entropy relative to a white noise signal. This relative entropy is called *negentropy* and is conceptually different to the negative spectral entropy later used for SEC_{FW} in Eq. (12). Li *et al.*[26] used this negentropy to determine signal onsets. While the proposed method is significantly better than the AIC picker, it requires a new empirical parameter for threshold setting to be identified from experience, which makes it tedious to apply to new applications. Without an explicit link to negentropy, Xu *et al.*[49] selected onsets in financial time series in an inconclusive manner by using the signal kurtosis instead of variance in the AIC picker, which is one of the weaker contrast functions used for ICA.[48] Other entropy measures, such as Tsallis entropy and permutation entropy, were also introduced in that paper, and the results showed similar behavior as the kurtosis-based AIC picker. Küperkoch *et al.*[50] combined signal kurtosis with the STA/LTA picker instead of the AIC picker. Using eight empirical parameters, they significantly outperform the classical STA/LTA picker. The derivative of entropy was used by Sabbione and Velis[51] along with two empirical parameters as an indicator of signal onset, giving satisfactory results that, unfortunately, were not compared to traditional onset pickers. In contrast to the present study, all of these entropy-based methods were applied to signals that were unknown *a priori*. Given the knowledge of the peak-like frequency spectrum of the expected signal, spectral entropy is used here instead.

To calculate spectral entropy,[52] a discrete power spectrum $S_{xx}(f)$ is used, which is calculated from the discrete Fourier transform $X(f)$ of a signal sequence $s(t)$:

$$S_{xx}(f) = |X(f)|^2 \tag{6}$$

with

$$X(f) = \sum_{t=0}^{N-1} s(t) e^{j(2\pi/N)ft}, \tag{7}$$

where N is the number of samples in the signal sequence, t is the sample index, and f is the Fourier component index.[53]

Its discrete frequencies, f are interpreted as the set of symbols and their probabilities are the normalized amplitudes $P(f)$ of the power spectrum:

$$P(f) = \frac{S_{xx}(f)}{\sum_f} S_{xx}(f). \tag{8}$$

Thus, the spectral entropy is

$$\hat{H}_s = -\sum_{i=1}^{m} P_i \log_2(P_i). \tag{9}$$

The normalized spectral entropy is then

$$H_s = \frac{\hat{H}_s}{\log_2(N)}. \tag{10}$$

Of all distributions in a finite interval, uniform distributions have the largest entropy.[54] If a distribution contains symbols that have larger probabilities than others, the entropy decreases to the point of a degenerate distribution with singular support that has entropy minimum.[55] Therefore, for ultrasound data, it is expected that $H_s \to 1$ for the first segment, which mainly contains white noise, and $H_s \to 0$ in the second segment, which contains a distinct frequency peak. Analogous to the BW function of the AIC picker, moving a window from the right across the waveform would generate a constant low result, since the window contains only the ultrasound pulse, up until the onset point where increasingly white noise is added, increasing H_s. This is shown in Fig. 3. Moving a window from the left across the waveform conversely produces a mirror image result compared to the AIC picker FW function, where H_s is constantly high while the window contains only white noise, and decreases when the window includes a portion of the

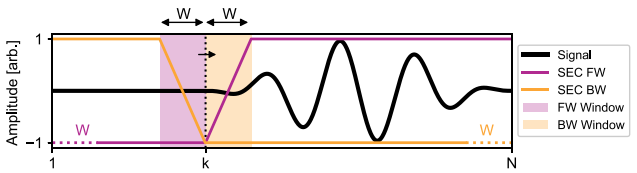

FIG. 3. (Color online) Schematic representation of the spectral entropy criterion (SEC) picker. While k is moved over the entire waveform, the FW and BW functions are calculated for signal windows of fixed length W preceding and following k, respectively. The dotted lines indicate sample points for which no SEC can be calculated as their distance to the start or end of the signal is less than the window length W. When these functions are added, the global minimum gives the signal onset predicted by the SEC.

ultrasonic signal. For convenience, a structure for the SEC picker is created that resembles the structure of the AIC picker and contains forward and backward running functions:

$$SEC_{FW}(k) = -H_s(t = [k - W - 1, k - 1]),$$
$$SEC_{BW}(k) = H_s(t = [k, k + W]). \tag{11}$$

Here, W is a constant window size in which H_s is evaluated, which is equal for both windows. Consequently, SEC_{FW} is defined only for $k > W$ and SEC_{BW} only for $k < N - W$. The deviation from the variable window size of the AIC picker was chosen since H_s is usually calculated from the DFT of a windowed signal, with a frequency resolution depending on the number of samples in that window, given zero-padding is not applied. Enforcing an equal and constant window size makes the results of the FW and BW functions comparable. To achieve behavior analogous to the AIC picker, in which a summation of the FW and BW function yields a global minimum at the signal onset point, SEC_{FW} contains the negative spectral entropy. Using Eqs. (6)–(10), the full SEC picker can be written as follows:

$$\begin{aligned}\mathrm{SEC}(k) &= SEC_{FW}(k) + SEC_{BW}(k)\\ &= -H_s(t = [k - W - 1, k - 1])\\ &\quad + H_s(t = [k, k + W]).\end{aligned} \tag{12}$$

This essentially just contains a set of operations performed on two sliding DFT windows that can be easily implemented with a few lines of code using a loop function. A more efficient implementation is described in Sec. V A 4.

IV. METHODS

To evaluate the performance of the SEC picker and compare it to the AIC picker, both synthetic signals and experimental data are used. This section describes how these data are generated.

For the synthetic signals, ultrasonic pulses were modeled as modified raised cosine (RCN) pulses. This type of pulse is usually generated by modulating a cosine signal with n_p periods with a cosine window and is a standard function for simulating ultrasonic pulses.[56,57] To increase the rather flat slope of the RCN functions after onset, they were modified to a cosine window sine function (RCSN) defined as

$$RCSN(t) = \begin{cases} \left(1 + \cos\dfrac{\omega_0}{n_p}t\right)\sin\omega_0 t, \\ \quad \text{for} -n_p\dfrac{\pi}{\omega_0} \le t \le n_p\dfrac{\pi}{\omega_0}, \\ 0 \quad \text{else}, \end{cases} \tag{13}$$

where ω_0 is the base frequency of the pulse, which is not important for the SEC by *per se*, since it only scales the width of the pulse. More important is the relation to the sampling frequency of the measurement, as shown in Sec. V A 2. Thus, only the number of samples N_T per wave period T is controlled, while the base frequency is fixed at $\omega_0 = 2\pi$. In order to simulate the onset of an acoustic signal, an RCS4 pulse (with $n_p = 4$) is generated, scaled to the range $[-1, 1]$, and appended to a zero vector of length $0.75N_T$. For all tests run on synthetic signals (Sec. V A), both scale and relative position in the signal were fixed for all RCS4 pulses. Gaussian noise was then added to the resulting waveform.

For correct onset picking, the global signal-to-noise ratio (SNR) is less significant than the noise relative to the pulse slope and the amplitudes immediately following the signal onset, since it aims at detecting the low amplitude start of a signal burst, which is not influenced by the global signal amplitude. Acknowledging that it reflects this relationship only partially, we define a more local SNR that relates the standard deviation of the white noise σ_w to the absolute amplitude of the first local extremum of the signal A_1, which has a value of $A_1 = -0.06$ for the RCS4 pulse:

$$SNR = \frac{|A_1|}{\sigma_w}. \tag{14}$$

Using this procedure of artificial pulse generation, Monte Carlo (MC) simulations were conducted with 10^4 trials. In these simulations, the SEC window width W, the number of samples per wave period N_T, and the SNR were varied. No further modifications were applied to the waveforms or the picker parameters. The results are discussed in Secs. V A 1–V A 3. Figure 4 shows a sample signal with SNR = 2 and $N_T = 200$. The SEC was applied using a window width of $W = N_T$. Although the forward and backward functions do not immediately change their behavior at the simulated onset point at sample 400, by adding their results according to Eq. (12), the global minimum is found with only one sample error.

In addition to simulations using synthetic signals, the SEC picker was also compared to the AIC picker using experimental ultrasonic data to verify its performance under more realistic conditions. The dataset was acquired at the Bundesanstalt für Materialforschung und Prüfung (BAM) (Federal Institute for Materials Research and Testing) as

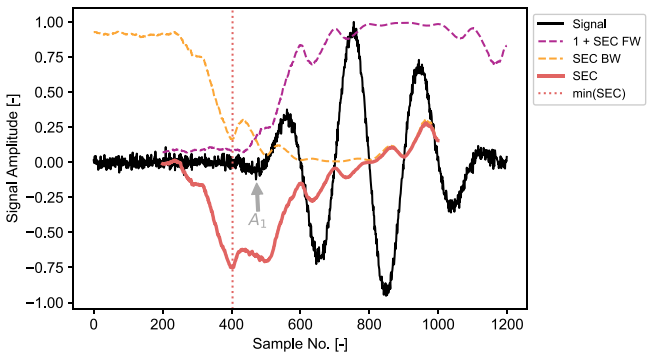

FIG. 4. (Color online) Exemplary synthetic signal ($W = T$, $N_T = 200$ samples/T, SNR = 2) for the MC simulations, including the SEC FW and BW functions, as well as their sum and the resulting signal onset. The location of first minimum of the RSC4 pulse is indicated as A_1.

https://doi.org/10.1121/10.0024337

part of an interlaboratory test initiated by Technische Universität Dresden.[58] The ultrasonic signal was acquired using a USG 40 ultrasound generator (Geotron Elektronik, Germany) at a sending frequency of 64 kHz in conjunction with Geotron UPG-D ultrasound transducers in a through-transmission setup. The ultrasonic signal was propagated through 18 concrete drill cores with a length of 200 mm and a width of 100 mm at varying radial positions, resulting in 216 waveforms containing 5000 samples, recorded at 10 MHz. More detailed information of the specimens and data acquisition procedure is given by Gebauer *et al.*[58] Onset times were manually picked for these waveforms to compare the SEC and AIC picker results.

V. RESULTS AND DISCUSSION

A. Monte-Carlo simulations using synthetic signals

1. Influence of window size

A major criticism of the AIC picker is its instability in relation to the size of the recorded signal snipped both before and after the true onset, which has resulted in the introduction of free parameters in both adaptations of the AIC picker (refer to Sec. II) and alternative onset pickers (refer to Sec. III). Thus, one of the performance requirements of the SEC picker is that it does not require any free parameters. Contrary to the AIC picker, the SEC picker does not include all samples in the computation, but only those covered by the moving windows, making their equal and fixed width the only free parameter. Before other performance characteristics can be evaluated, an optimal choice to constrain this parameter needs to be found. For this purpose, the window width was varied while the sampling rate and SNR were kept constant with $N_T = 150$ and SNR $= 8.6$. Figure 5 shows that the onset picking error as a function of W follows a periodic sawtooth-like behavior with a frequency of $2f_c$. In this behavior, crossings of the zero-error line occur at integer multiples of $T/2$ and $2T/3$. However, only the former are characterized by a very narrowband distribution, as indicated by the interdecile ratio (IDR):

$$IDR = p_{0.9} - p_{0.1}. \tag{15}$$

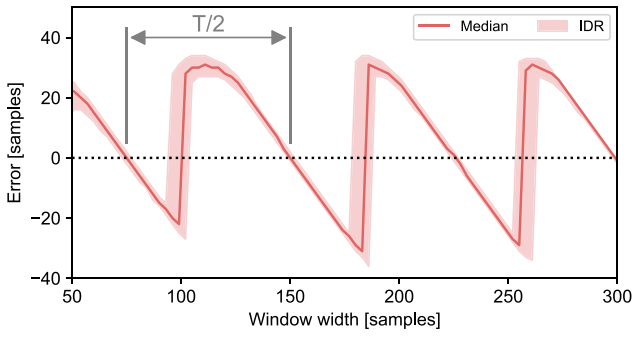

FIG. 5. (Color online) SEC onset picking error as a function of window width. The zero crossings occur exactly at multiples of the $T/2$ half-period of the RCS4 synthetic pulse.

Here, $p_{0.1}$ and $p_{0.9}$ are the first and ninth deciles of the distributions of the results of the MC simulations. The range of promising window width parameters can thus be narrowed down to

$$W = \frac{mT}{2}, \tag{16}$$

where m is a positive integer. In practice, therefore, the parameter W may not be considered as a free parameter anymore, since it is constrained by the transducer characteristics and sample frequency used. Thus, not only the modeling concept itself, but also the choice of parameters is based on prior knowledge. The only arbitrary component of the window width is the integer factor m. However, since a large m would require a large signal length before and after the true onset (see Fig. 3), choosing a low single-digit m value is advisable. For convenience, in the remainder of this study, the window width is chosen to be $m = 2$, so that $W = T$.

2. Influence of the sampling rate

Defining the required number of samples to be included in the spectral entropy calculation windows, only in relation to the dominant period, is not sufficient to characterize the quality of results alone—since the actual number of samples included is then also a function of the sampling rate. According to the Nyquist sampling theorem, more than two samples per period must be recorded for the waveform to be faithfully reconstructed from its Fourier components. However, since spectral entropy is calculated from the Fourier transform, the number of Fourier components is additionally related to the amount of information entering the calculation in Eq. (9). The SEC picker is based on the assumption that the first signal segment contains a mainly flat white noise spectrum, resulting in $H_s \to 1$ (refer to Sec. III). However, this behavior might not be reflected in the spectrum when it contains only a small number of Fourier components. Due to the stochastic behavior of the measured samples, the Fourier components may not form a flat distribution so that this assumption may not hold. As a result, the contrast between FW and BW function, and with it the onset picking quality, may deteriorate. Thus, the spectral resolution, being a function of the number of samples n_w included in each evaluation window, may influence the onset picking quality of the proposed SEC picker.

To investigate its influence using a MC simulation, the number of samples in the evaluation window n_w is varied while choosing a constant window width of $W = T$ and SNR $= 8.6$. Figure 6 shows the results from the MC simulation. Since the window width is equal to the fundamental period of the pulse, the given sampling rate N_T is equal to the number of samples included in each evaluation window n_w. The results of the SEC picker are compared to those of the AIC picker. They show that the SEC picker exhibits higher errors of onset picks than the AIC picker at low sampling rates, including higher fluctuation in results. The median results of the SEC picker outperform the AIC picker

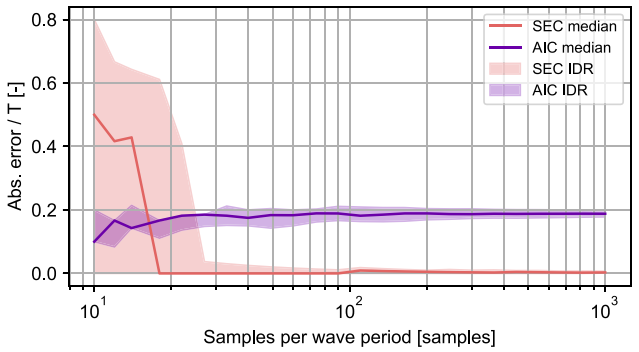

FIG. 6. (Color online) Absolute onset picking error of SEC and AIC pickers as a function of samples per wave period using a synthetic RCS4 pulse.

from a sampling rate of 18 samples/T and reach almost zero errors. A sampling rate of 18 samples/T results in only nine Fourier components per evaluation window. At this order of components, one outlier may drastically shift the result of Eq. (9). Starting from 27 samples/T, the main part of the SEC distribution has lower errors than the median of the AIC in this simulation. These results show that significant oversampling of the recorded signal is required for the SEC picker to outperform the AIC picker. When this oversampling is achieved, the SEC picker exhibits a very low error rate with very little variation. However, it is not possible to define a minimum oversampling required to achieve such accuracy, as further experiments have shown that it is additionally influenced by the noise level. Higher noise levels require higher oversampling.

3. Influence of noise

To assess the performance of the SEC picker in the presence of noise, the background noise was varied over the whole synthetic signal snippet. Figure 7 shows the onset picking error of the SEC picker compared to that of the AIC picker. In this MC simulation, the window width was fixed at $W = T$ and a high sampling rate of 150 samples/T was chosen. The results show that the median AIC picker error decreases continually from 82 samples to three samples with increasing SNR, starting from SNR = 4.5. The SEC picker error remains flat at one sample error starting from SNR = 2.8. When reducing SNR below these respective

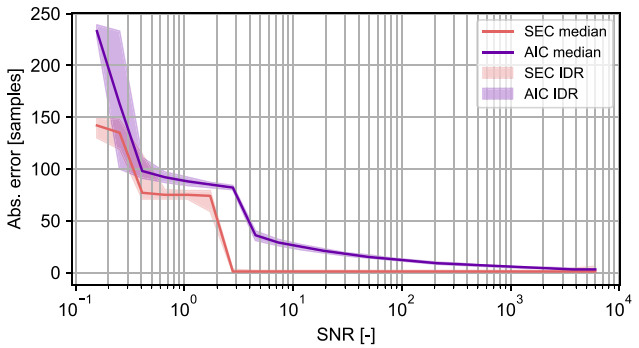

FIG. 7. (Color online) Absolute onset picking error of SEC and AIC pickers as a function of Gaussian noise added to the synthetics RCS4 pulse.

levels, both pickers exhibit step increases of the picking error. These step increases are likely a result of the algorithms completely missing the onset and treating the following half period of the signal as part of the noise. When the signal is drowned out by the noise like this, only the second half period of the signal after the first zero crossing is recognized as distinct from the noise. The error steps are thus half period shifts of the true onset. Although this is the case for both the AIC and SEC pickers, Fig. 7 shows that the SEC picker outperforms the AIC picker at all SNR levels, given an appropriate window width and high sampling rate.

4. Computational efficiency

In general, the concept of the SEC picker is easy to implement using moving windows, where a Fourier transform is first performed and then the spectral entropy is calculated. However, it is expected that calculating a large number of Fourier transforms is computationally expensive. To reduce the computational load, the SEC picker can be implemented using highly efficient implementations of the *spectrogram* function, which are available as packages for many higher programming languages. Here, the Python SciPy package[59] is used. The spectral power calculation for further entropy calculation can be conducted by setting the spectrogram function to give an output that is not frequency normalized, a boxcar window function, a window width of W, and a window overlap of $W - 1$. Furthermore, this spectrogram, and subsequently the spectral entropy, only needs to be calculated once, since the forward SEC function at sample k is the same as the backward SEC function at sample $k - W$ (see Fig. 3). After the calculation of the forward function is performed, the results only need to be shifted to obtain the backward function.

To benchmark the execution time, the SEC and AIC pickers in Python were compared using the *process_time* function of the *time* package on a standard laptop personal computer with an Intel Core i5-8250U CPU (Intel Corp., Santa Clara, CA) at 1.6GHz and 8 GB RAM, using a 64 bit Windows 10 operating system (Microsoft Corp., Redmond, WA). To provide a relational comparison of the computational cost, the SEC picker was tested against two implementations of AIC picker. The first was a naive implementation in which Eq. (4) is simply looped over the whole signal. This is an obvious implementation that has been used repeatedly in the literature.[60,61] The second AIC implementation is part of the open source package *vallenae 0.7.0*[62] and is based on *numba*.[63] Given its easy accessibility, this implementation was preferred over the algorithm proposed by Long *et al.*,[64] which also aims to improve the execution time of the AIC picker. While both AIC pickers and the SEC picker were tested for varying signal lengths [Fig. 8(a)], the SEC picker was also tested for varying window widths [Fig. 8(b)].

The results show that the mean execution time of the SEC picker increases almost linearly with the signal length [Fig. 8(a)] and the window width [Fig. 8(b)]. This is the

https://doi.org/10.1121/10.0024337

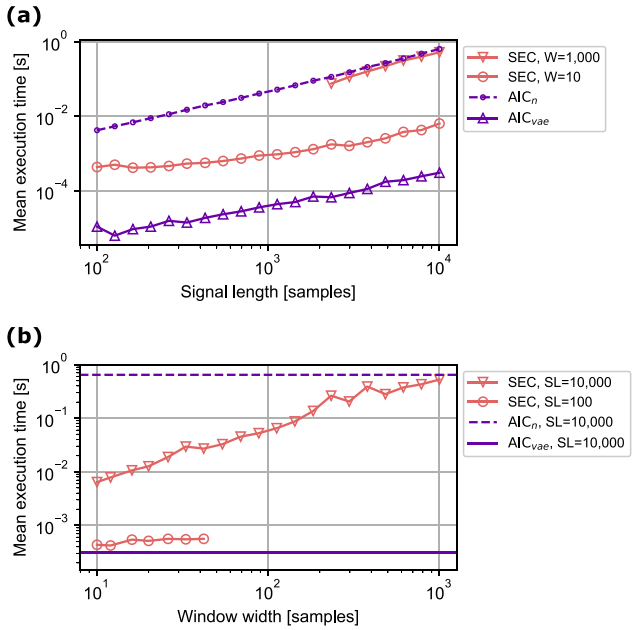

FIG. 8. (Color online) Mean execution time of the SEC and AIC pickers. If the signal length $\leq 2W$, no SEC can be calculated. The AIC picker performance is evaluated for a naive (n) and an optimized (vae) implementation. (a) Execution time as a function of signal length, (b) execution time as a function of W, which varies only for the SEC picker.

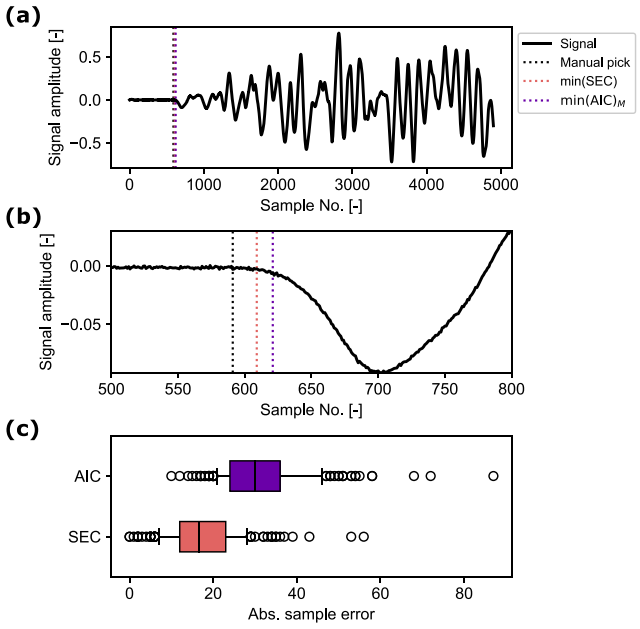

FIG. 9. (Color online) Experimental verification of the SEC picker: (a) exemplary through-transmission signal with marked onset as found by manual picking, the SEC picker, and the AIC picker; (b) section of signal shown in (a), zoomed in to the onset region; (c) absolute errors of both pickers compared to the manual picks for the whole dataset.

case, especially for high values of the respective other parameters, while the execution time increases more slowly in the lower range. The execution times could not be calculated for all parameter combinations, since for the SEC picker, a smaller signal length needs to be at least twice the window width. When comparing with the AIC picker, the results show that the SEC picker executes faster than a naive implementation of the AIC picker. However, an optimized implementation of the AIC picker is significantly more efficient than the SEC picker, executing three orders of magnitude faster for long signals and wide windows.

B. Verification on experimental data

After the successful numerical trials with the SEC picker, its performance was tested on experimental data for which the signal onsets were manually picked. Figures 9(a) and 9(b) show an example signal from the dataset with the manual pick and the AIC and SEC picks marked. Since the sampling frequency of the data acquisition system and the transducer center frequency are known, the SEC window width can be set accordingly. In this case, the window width is set to one period, so the window width of $W = 156$ samples additionally represents a dense sampling. Figure 9(c) shows the results of both the SEC picker and the AIC picker for the whole dataset. While the AIC picker has a median error of 30 samples with a spread of $IDR = 25$ samples, the SEC picker produces a median error of only 17 samples with a spread of $IDR = 21$ samples. With a comparable deviation from the median, the results show that SEC picker outperforms the AIC picker also for the given experimental data. The reduction in SEC performance advantage compared to simulation results is likely caused by the signal spectrum containing more than a single frequency, resulting in a bell-shaped frequency distribution. Thus, the optimal window length cannot be set, which may cause onset picking errors (refer to Sec. V A 1). Additionally, the spectral entropy contrast between the white noise segment of the waveform and the dominant frequency pulse is reduced, which may increase sensitivity to spectral variations and subsequently reduce accuracy. Similar behavior is expected when the SEC is applied to reflection measurements in scattering media. In this case, the first waveform segment may deviate from the white noise assumption made in Sec. III since scatterers cause early reflections of the sent signal, resulting in a spectral peak in this segment. This is also expected to reduce the spectral entropy contrast between the signal segments, which persists due to the low SNR in the segment preceding the onset.

VI. CONCLUSIONS

We present a new signal onset picker specifically designed for ultrasonic measurements, based on the calculation of the spectral entropy of signal segments to separate segments containing the ultrasonic pulse from segments containing only white noise. This SEC picker was developed because the commonly used AIC picker in Maeda's formulation was based on inappropriate assumptions. Additionally, Maeda's AIC picker was initially designed to detect previously unknown signals, so the prior knowledge available in ultrasonic measurements was not included in the algorithm. The presented SEC picker is based on the assumption that the received ultrasonic pulse has low

spectral entropy, i.e., the signal spectrum contains only few dominant frequency peaks, contrary to the wideband noise preceding the pulse. Based on this assumption, the method follows the general moving-window approach of the AIC picker. Monte-Carlo simulations have shown that the arbitrary window width parameter can be reasonably restricted to a low single-digit positive integer, so that the method has virtually no free parameters. Furthermore, simulations have shown that the SEC picker performs best when the sampling rate is at least about 1 order of magnitude higher than Nyquist frequency. If this condition is satisfied, the SEC picker outperforms the AIC picker on synthetic signals at all SNR levels tested while being computationally more efficient than naive implementations of the AIC picker. Application to an experimental dataset of ultrasonic through-transmission measurements has shown that the SEC picker outperforms the AIC picker also in real-life settings. For both synthetic and real ultrasonic through-transmission data, the SEC picker presented here provides a significant improvement in automated signal onset picking over the current standard AIC picker due to its efficient implementation and higher accuracy for densely sampled data. In future research, these promising results should be further validated in different ultrasonic through-transmission applications, such as damage detection or monitoring of material properties, using both experimental and numerical setups, to enable adaption of this easy-to-use method in real-world use cases. Additionally, future research should use the analysis of the flawed premises of Maeda's AIC picker to develop onset pickers for further domains, such as ultrasonic pitch-catch measurements, acoustic emission testing, or geophysical applications. Similar to the SEC picker for ultrasonic through-transmission testing, these onset pickers should be tailored to their respective domain while remaining simple, robust, and conceptually sound.

ACKNOWLEDGMENTS

We thank N. Aßmann (BAM 8.2) for generating the experimental data shown in this paper. We also thank S. Küttenbaum (BAM 8.2) for fruitful discussions on the AIC picker. Special thanks go to O. Dahlman (OD Science Applications, Sweden) and S. Mykkeltveit (NORSAR, Norway) for taking the effort to search their archives for a hard copy of Ref. 19 that previously seemed untraceable.

AUTHOR DECLARATIONS

Conflict of Interest

The authors have no conflicts to disclose.

Author Contributions

Benjamin Bühling: Conceptualization, methodology, software, validation, formal analysis, investigation, data curation, writing – original draft, visualization, supervision, project administration. Stefan Maack: Validation, investigation, resources, data curation, writing – review & editing.

DATA AVAILABILITY

The data that support the findings of this study are available from the corresponding author upon reasonable request.

[1]N. Karamzadeh, G. J. Doloei, and A. M. Reza, "Automatic earthquake signal onset picking based on the continuous wavelet transform," IEEE Trans. Geosci. Remote Sens. **51**(5), 2666–2674 (2013).
[2]B. Bergfeld, A. van Herwijnen, G. Bobillier, E. Larose, L. Moreau, B. Trottet, J. Gaume, J. Cathomen, J. Dual, and J. Schweizer, "Crack propagation speeds in weak snowpack layers," J. Glaciol. **68**(269), 557–570 (2022).
[3]A. Carpinteri, J. Xu, G. Lacidogna, and A. Manuello, "Reliable onset time determination and source location of acoustic emissions in concrete structures," Cem. Concr. Compos. **34**(4), 529–537 (2012).
[4]C. Li, L. Huang, N. Duric, H. Zhang, and C. Rowe, "An improved automatic time-of-flight picker for medical ultrasound tomography," Ultrasonics **49**(1), 61–72 (2009).
[5]G. Jin, H. Zhu, D. Jiang, J. Li, L. Su, J. Li, F. Gao, and X. Cai, "A signal-domain object segmentation method for ultrasound and photoacoustic computed tomography," IEEE Trans. Ultrason. Ferroelectr. Freq. Control **70**(3), 253–265 (2023).
[6]J. H. Kurz, C. U. Grosse, and H.-W. Reinhardt, "Strategies for reliable automatic onset time picking of acoustic emissions and of ultrasound signals in concrete," Ultrasonics **43**(7), 538–546 (2005).
[7]F. Suñol, D. A. Ochoa, and J. E. Garcia, "High-precision time-of-flight determination algorithm for ultrasonic flow measurement," IEEE Trans. Instrum. Meas. **68**(8), 2724–2732 (2019).
[8]B. Bühling, S. Küttenbaum, S. Maack, and C. Strangfeld, "Development of an accurate and robust air-coupled ultrasonic time-of-flight measurement technique," Sensors **22**(6), 2135 (2022).
[9]J. C. Jackson, R. Summan, G. I. Dobie, S. M. Whiteley, S. G. Pierce, and G. Hayward, "Time-of-flight measurement techniques for airborne ultrasonic ranging," IEEE Trans. Ultrason. Ferroelectr. Freq. Control **60**(2), 343–355 (2013).
[10]S. Dencks, R. Barkmann, F. Padilla, P. Laugier, G. Schmitz, and C. C. Gluer, "Model-based estimation of quantitative ultrasound variables at the proximal femur," IEEE Trans. Ultrason. Ferroelectr. Freq. Control **55**(6), 1304–1315 (2008).
[11]H. Ping, "Simulation of ultrasound pulse propagation in lossy media obeying a frequency power law," IEEE Trans. Ultrason. Ferroelectr. Freq. Control **45**(1), 114–125 (1998).
[12]T. P. Philippidis and D. G. Aggelis, "Experimental study of wave dispersion and attenuation in concrete," Ultrasonics **43**(7), 584–595 (2005).
[13]S. Küttenbaum, "Zur validierung von zerstörungsfreien messverfahren für die probabilistische beurteilung von bestandsbauwerken mit gemessenen daten" ("Validation of non-destructive measurement procedures for reliability assessments of existing structures using measured data"), Ph.D. thesis, Universität Der Bundeswehr München, Munich, Germany, 2021, https://athene-forschung.unibw.de/139481.
[14]V. K. Kachanov, I. V. Sokolov, M. A. Karavaev, and R. V. Kontsov, "Selecting optimum parameters of ultrasonic noncontact shadow method for testing products made of polymer composite materials," Russ. J. Nondestruct. Test. **56**(10), 831–842 (2020).
[15]E. Niederleithinger, J. Wolf, F. Mielentz, H. Wiggenhauser, and S. Pirskawetz, "Embedded ultrasonic transducers for active and passive concrete monitoring," Sensors **15**(5), 9756–9772 (2015).
[16]L. Espinosa, J. Bacca, F. Prieto, P. Lasaygues, and L. Brancheriau, "Accuracy on the time-of-flight estimation for ultrasonic waves applied to non-destructive evaluation of standing trees: A comparative experimental study," Acta Acust. united Acust **104**(3), 429–439 (2018).
[17]H. Akaike, "Information theory and an extension of the maximum likelihood principle," in *Selected Papers of Hirotugu Akaike*, edited by E. Parzen, K. Tanabe, and G. Kitagawa (Springer, New York, 1998), pp. 199–213.
[18]G. Kitagawa and H. Akaike, "A procedure for the modeling of non-stationary time series," Ann. Inst. Stat. Math. **30**(2), 351–363 (1978).
[19]GSE/JAPAN/40, "A fully automated method for determining the arrival times of seismic waves and its application to an on-line processing system," in *34th Session of the Ad Hoc Group of Scientific Experts to*

Consider International Cooperative Measures to Detect and Identify Seismic Events, (GSE, Geneva, Switzerland, 1992), pp. 1–45, GSE/RF/62.
[20]R. V. Allen, "Automatic earthquake recognition and timing from single traces," Bull. Seismol. Soc. Am. **68**(5), 1521–1532 (1978).
[21]J. Akram and D. W. Eaton, "A review and appraisal of arrival-time picking methods for downhole microseismic data," Geophysics **81**(2), KS71–KS91 (2016).
[22]P. Sedlak, Y. Hirose, and M. Enoki, "Acoustic emission localization in thin multi-layer plates using first-arrival determination," Mech. Syst. Signal Process. **36**(2), 636–649 (2013).
[23]N. Maeda, "A method for reading and checking phase time in auto-processing system of seismic wave data," Zisin (J. Seismol. Soc. Jpn.) **38**(3), 365–379 (1985) (in Japanese).
[24]K. Kuge, "Source modeling using strong-motion waveforms: Toward automated determination of earthquake fault planes and moment-release distributions," Bull. Seismol. Soc. Am. **93**(2), 639–654 (2003).
[25]H. Zhang, C. Thurber, and C. Rowe, "Automatic P-wave arrival detection and picking with multiscale wavelet analysis for single-component recordings," Bull. Seismol. Soc. Am. **93**(5), 1904–1912 (2003).
[26]Y. Li, Z. Ni, and Y. Tian, "Arrival-time picking method based on approximate negentropy for microseismic data," J. Appl. Geophys. **152**, 100–109 (2018).
[27]K. Aggarwal, S. Mukhopadhya, and A. K. Tangirala, "A prediction framework with time-frequency localization feature for detecting the onset of seismic events," PLoS One **16**(4), e0250008 (2021).
[28]M. Elfering, S. Annas, H.-A. Jantzen, and U. Janoske, "Method for time-of-flight estimation of low frequency acoustic signals in reverberant and noisy environment with sparse impulse response," Meas. Sci. Technol. **33**(4), 045101 (2022).
[29]A. Hendriyana, "Detection and Kirchhoff-type migration of seismic events by use of a new characteristic function," Ph.D. thesis, Universität Potsdam, Potsdam, Germany, 2017, https://publishup.uni-potsdam.de/frontdoor/index/index/docId/39887.
[30]A. K. Das and C. K. Y. Leung, "A new power-based method to determine the first arrival information of an acoustic emission wave," Struct. Health Monit **18**(5-6), 1620–1632 (2018).
[31]A. K. Das and C. K. Y. Leung, "ICD: A methodology for real time onset detection of overlapped acoustic emission waves," Autom. Constr. **119**, 103341 (2020).
[32]Y. Bao and J. Jia, "Improved time-of-flight estimation method for acoustic tomography system," IEEE Trans. Instrum. Meas. **69**(4), 974–984 (2020).
[33]Y. Tan, C. He, J. Yu, and G. Feng, "A combined method for automatic microseismic event detection and arrival picking," in *SEG Technical Program Expanded Abstracts 2014* (Society of Exploration Geophysicists, Denver, CO, 2014), pp. 2335–2340.
[34]T. Shen, X. Tuo, H. Li, Y. Liu, and W. Rong, "A first arrival picking method of microseismic data based on single time window with window length independent," J. Seismol. **22**(6), 1613–1627 (2018).
[35]H. Li, Z. Yang, and W. Yan, "An improved AIC onset-time picking method based on regression convolutional neural network," Mech. Syst. Signal Process. **171**, 108867 (2022).
[36]E. Landis, C. Ouyang, and S. P. Shah, "Automated determination of first p-wave arrival and acoustic emission source location," J. Acoust. Emiss. **10**(1-2), S97–S103 (1991), http://www.aewg.org/jae/JAE-Vol_10-1991.pdf.
[37]F. Bai, D. Gagar, P. Foote, and Y. Zhao, "Comparison of alternatives to amplitude thresholding for onset detection of acoustic emission signals," Mech. Syst. Signal Process. **84**, 717–730 (2017).
[38]J. Münchmeyer, J. Woollam, A. Rietbrock, F. Tilmann, D. Lange, T. Bornstein, T. Diehl, C. Giunchi, F. Haslinger, D. Jozinović, A. Michelini, J. Saul, and H. Soto, "Which picker fits my data? a quantitative evaluation of deep learning based seismic pickers," JGR. Solid Earth **127**(1), e2021JB023499 (2022).
[39]J. deLeeuw, "Introduction to akaike (1973) information theory and an extension of the maximum likelihood principle," in *Breakthroughs in Statistics: Foundations and Basic Theory*, edited by S. Kotz and N. L. Johnson (Springer, New York, 1992), pp. 599–609.
[40]K. Aho, D. Derryberry, and T. Peterson, "Model selection for ecologists: The worldviews of AIC and BIC," Ecology **95**(3), 631–636 (2014).
[41]M. Leonard and B. L. N. Kennett, "Multi-component autoregressive techniques for the analysis of seismograms," Phys. Earth Planet. Inter **113**(1), 247–263 (1999).
[42]R. Sleeman and T. van Eck, "Robust automatic p-phase picking: An online implementation in the analysis of broadband seismogram recordings," Phys. Earth Planet. Inter. **113**(1), 265–275 (1999).
[43]C. E. Shannon, "A mathematical theory of communication," Bell Syst. Tech. J **27**(3), 379–423 (1948).
[44]S. Bhooshan, "Introduction to information theory," in *Fundamentals of Analogue and Digital Communication Systems*, Lecture Notes in Electrical Engineering (Springer, Singapore, 2022), Vol. 785, p. 517–558.
[45]S. L. E. F. da Silva and G. Corso, "Microseismic event detection in noisy environments with instantaneous spectral Shannon entropy," Phys. Rev. E **106**(1), 014133 (2022).
[46]A. K. Das and C. K. Y. Leung, "Power spectral entropy of acoustic emission signal as a new damage indicator to identify the operating regime of strain hardening cementitious composites," Cem. Concr. Compos. **104**, 103409 (2019).
[47]A. K. Das, J. Qiu, C. K. Y. Leung, and J. Yu, "A novel strategy to assess healing induced recovery of mechanical properties (HIRMP) of strain hardening/engineering cementitious composites (SHCCS/ECCS) in autogenous healing," Cem. Concr. Compos. **142**, 105177 (2023).
[48]A. Hyvärinen, J. Karhunen, and E. Oja, "Information theory," in *Independent Component Analysis* (John Wiley & Sons, Ltd, New York, 2001), pp. 105–124.
[49]S. Xu, M. Shao, W. Qiao, and P. Shang, "Generalized AIC method based on higher-order moments and entropy of financial time series," Phys. A: Stat. Mech. Appl. **505**, 1127–1138 (2018).
[50]L. Küperkoch, T. Meier, J. Lee, W. Friederich, and EGELADOS Working Group, "Automated determination of *P*-phase arrival times at regional and local distances using higher order statistics," Geophys. J. Int. **181**(2), 1159–1170 (2010).
[51]J. I. Sabbione and D. Velis, "Automatic first-breaks picking: New strategies and algorithms," Geophysics **75**(4), V67–V76 (2010).
[52]B. Boashash, G. Azemi, and N. Ali Khan, "Principles of time–frequency feature extraction for change detection in non-stationary signals: Applications to newborn EEG abnormality detection," Pattern Recognit. **48**(3), 616–627 (2015).
[53]A. V. Oppenheim and R. W. Schafer, "Computation of the discrete fourier transform," in *Discrete-Time Signal Processing*, 2nd ed., Prentice-Hall signal processing series (Prentice-Hall, Upper Saddle River, NJ, 1999), pp. 629–692.
[54]O. Calin and C. Udrişte, "Maximum entropy distributions," in *Geometric Modeling in Probability and Statistics* (Springer International Publishing, Cham, Switzerland, 2014), pp. 165–187.
[55]T. O. Kvålseth, "Variation for categorical variables," in *International Encyclopedia of Statistical Science*, edited by M. Lovric (Springer, Berlin, Heidelberg, 2011), pp. 1642–1645.
[56]K.-J. Langenberg, R. Marklein, and K. Mayer, "Mathematical foundations," in *Ultrasonic Nondestructive Testing of Materials: Theoretical Foundations* (CRC Press, Boca Raton, FL, 2012), pp. 13–85.
[57]A. Asadollahi and L. Khazanovich, "Analytical reverse time migration: An innovation in imaging of infrastructures using ultrasonic shear waves," Ultrasonics **88**, 185–192 (2018).
[58]D. Gebauer, R. E. Beltrán Gutiérrez, S. Marx, M. Butler, K. Grahl, T. Thiel, S. Maack, S. Küttenbaum, S. Pirskawetz, W. Breit, M. Schickert, and M. Krüger, "Interrelated dataset of rebound numbers, ultrasonic pulse velocities and compressive strengths of drilled concrete cores from an existing structure and new fabricated concrete cubes," Data Brief **48**, 109201 (2023).
[59]P. Virtanen, R. Gommers, T. E. Oliphant, M. Haberland, T. Reddy, D. Cournapeau, E. Burovski, P. Peterson, W. Weckesser, J. Bright, S. J. van der Walt, M. Brett, J. Wilson, K. J. Millman, N. Mayorov, A. R. J. Nelson, E. Jones, R. Kern, E. Larson, C. J. Carey, İ. Polat, Y. Feng, E. W. Moore, J. VanderPlas, D. Laxalde, J. Perktold, R. Cimrman, I. Henriksen, E. A. Quintero, C. R. Harris, A. M. Archibald, A. H. Ribeiro, F. Pedregosa, and P. van Mulbregt, and SciPy 1.0 Contributors, "SciPy 1.0: Fundamental algorithms for scientific computing in Python," Nat. Methods **17**, 261–272 (2020).
[60]A. Hotovec-Ellis and C. Jeffries, "Near real-time detection, clustering, and analysis of repeating earthquakes: Application to Mount St. Helens and redoubt volcanoes," in *Seismological Society of America Annual Meeting*, Reno, Nevada (April 20, 2016), https://github.com/ahotovec/REDPy (Last viewed January 12, 2024).

[61]E. V. Cano, J. Akram, and D. B. Peter, "Automatic seismic phase picking based on unsupervised machine-learning classification and content information analysis," Geophysics **86**(4), V299–V315 (2021).
[62]Vallen Systeme, Information on Vallen ae python tools v. 0.7.0 available at https://github.com/vallen-systems/pyVallenAE (Last viewed 2022).
[63]S. K. Lam, A. Pitrou, and S. Seibert, "Numba: A LLVM-based Python JIT compiler," in *Proceedings of the Second Workshop on the LLVM Compiler Infrastructure in HPC*, Austin, TX (Association for Computing Machinery, New York, 2015), pp. 1–6 (Last viewed January 12, 2024).
[64]Y. Long, J. Lin, B. Li, H. Wang, and Z. Chen, "Fast-AIC method for automatic first arrivals picking of microseismic event with multitrace energy stacking envelope summation," IEEE Geosci. Remote Sens. Lett. **17**(10), 1832–1836 (2020).